Steel and Composite Structures, *Vol. 38, No. 4 (2021) 463-476*
DOI: https://doi.org/10.12989/scs.2021.38.4.463

Improved analytical formulation for Steel-Concrete (SC) composite walls under out-of-plane loads

Saeid Sabouri-Ghomi[1a], Arman Nasri[1b], Younes Jahani[2c] and Anjan K. Bhowmick*[3]

[1]*Civil Engineering Department, K.N. Toosi University of Technology, Tehran, Iran*
[2]*Analysis and Advanced Materials for Structural Design (AMADE), Polytechnic School, University of Girona, Girona, Spain*
[3]*Department of Building, Civil and Environmental Engineering, Concordia University, Montreal, Canada*

(*Received June 12, 2020, Revised January 29, 2021, Accepted February 10, 2021*)

Abstract. The concept of using Steel-concrete (SC) composite walls as retaining walls has recently been introduced by the authors and their effectiveness of resisting out-of-plane loads has also been demonstrated. In this paper, an improved analytical formulation based on partial interaction theory, which has previously been developed by the authors, is presented. The improved formulation considers a new loading condition and also accounts for cracking in concrete to simulate the real conditions. Due to a limited number of test specimens, further finite element (FE)simulations are performed in order to verify the analytical procedure in more detail. It is observed that the results from the improved analytical procedure are in excellent agreement with both experimental and numerical results. Moreover, a detailed parametric study is conducted using the developed FE model to investigate effects of different parameters, such as distance between shear connectors, shear connector length, concrete strength, steel plate thickness, concrete cover thickness, wall's width to thickness ratio, and wall's height to thickness ratio, on the behavior of SC composite walls subjected to out-of-plane loads.

Keywords: SC composite wall; out-of-plane loads; partial interaction theory; finite element analysis; experimental test; retaining wall

1. Introduction

Deep excavation is utilized in tall buildings for many reasons, such as to reach the proper bedrock, to provide parking space for vehicles, to improve the architecture space, etc. In some cases, the depth of excavation exceeds 50 meters. During the excavation process, simplified methods such as nailing are utilized against soil movements. This simplified method is neither permanent nor efficient and may lose its resistance after earthquakes, landslides, etc. Therefore, retaining walls are utilized in construction to resist soil pressure. While reinforced concrete retaining walls are commonly used in construction projects, the need for huge temporary formworks, high dense reinforcing, low construction speed, engaging a large number of workers, etc. is some of the disadvantages of this system (Yan *et al.* 2018, Qin *et al.* 2019).

To overcome the disadvantages of the reinforced concrete walls mentioned above, composite (steel-concrete) wall is proposed by the authors to use as a retaining wall (Sabouri-Ghomi *et al.* 2020). This system contains one steel plate, concrete cover, shear connectors, and thermal reinforcing networks. The concrete cover is attached to the steel plate using shear connectors. The concrete cover is in the vicinity of soil and steel plate.

In other words, the steel plate acts not only as a component of the composite wall but is also utilized as permanent formwork. Therefore, the composite system can address all of the disadvantages of reinforced concrete walls and at the same time, the construction speed will increase and costs will decrease significantly. The general configuration of this system is shown in Fig. 1.

The shear connectors have an important role in composite walls. By increasing the number of shear connectors, the slip between layers can be decreased. There are different shapes of shear connectors; hooked shape, studs, etc. The shear connectors are welded to the steel plate to prevent any slip between the layers (Fig. 1). Also, they act as shear reinforcement for the out-of-plane loading.

A number of studies have been conducted on composite systems. Solomon *et al.* (1976) carried out various tests on composite beams and slabs and determined the failure mode in different conditions. Their study showed that the ACI and ASCE equations provide a conservative estimate of ultimate loads for sandwich beams.

Oduyemi and Wright (1989) presented different experimental tests on sandwich composite beams to identify the failure modes. They found that reducing the distance between the shear connectors could prevent steel plate from buckling and decrease the slip between layers. Subedi and Coyle (2002) enhanced the behavior of sandwich composite

*Corresponding author, Ph.D.
E-mail: anjan.bhowmick@concordia.ca
[a]Professor
E-mail: sabouri@kntu.ac.ir
[b]Ph.D. Student
E-mail: anasri@mail.kntu.ac.ir
[c]Ph.D. Student
E-mail: younes.jahani@yahoo.com

http://www.techno-press.org/?journal=scs&subpage=8
ISSN: 1229-9367 (Print), 1598-6233 (Online)

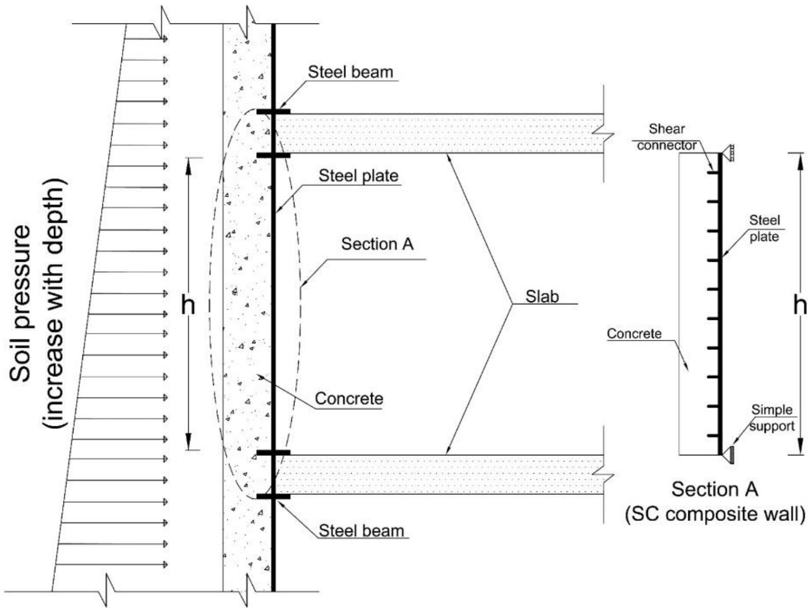

Fig. 1 General configuration of SC composite wall

beams by changing the roughness of the steel plate. Xie *et al.* (2005) investigated the static behavior of the friction-welded connections in composite beams. Three failure modes were observed in the push tests: plate tearing, shear failure through the cross-section of the bar, and failure across the bar/plate interface.

The experimental results were utilized to obtain an empirical equation for predicting the shear strength of embedded connections. In the other study, Xie *et al.* (2007) also conducted experimental and theoretical studies to investigate the behavior of sandwich composite beams. Four elementary modes: tension plate yielding, bar shear, bar tension, and concrete shear were observed in the specimens. Furthermore, it was concluded that the steel plate needs to be yielded in the tension side of the beams to have a ductile failure mode.

Liew and Sohel (2009) and Sohel and Liew (2011) utilized hooked shape shear connectors in composite beams and slabs. Their study showed that the distance between shear connectors should be at least equal to the concrete thickness in Steel-Concrete-Steel (SCS) composite beams. Vasdravellis *et al.* (2012) conducted experimental testing and numerical simulations to investigate the behavior of composite beams under flexural and compressive loads and proposed a simplified design model to use in engineering practice. Their study showed that compressive loading could lead to local buckling failure modes in the compression zones of a composite section. Dogan and Roberts (2010) compared experimental results of sandwich beams with full and partial interaction theories. Good agreement was observed between experimental data and the theoretical results based on partial interaction theory.

Partial interaction theory was utilized by many researchers to analyze the composite beams (Ranzi *et al.* 2003, Ranzi 2006, Cas *et al.* 2004). Cas *et al.* (2004) proposed a new strain-based finite element formulation for composite beams considering partial interaction theory. The accuracy of the formulation was evaluated by comparing numerical results with experimental results. Ding *et al.* (2016) studied the flexural stiffness of composite beams under a positive moment through combined experimental, numerical, and different standard methods. Fanaie *et al.* (2015) performed an analytical investigation on composite beams with different arrangements of shear connectors.

Yan *et al.* (2014) proposed theoretical methods to predict the tensile resistance of the J-hook connectors. The proposed methods were validated against experimental results. In another study, Yan *et al.* (2018) conducted 11 push-out tests and 11 tensile tests to evaluate the ultimate shear and tensile behavior of the headed stud. Analytical models were developed to predict the stud's behavior. Good agreement was observed between experimental results and the developed analytical models. Furthermore, Yan *et al.* (2015) experimentally studied 22 steel-concrete-steel (SCS) sandwich composite beams with different concrete batches and different connectors. From these tests, it was found that the angle connectors could not prevent uplifting due to weak pullout resistance. Also, Yan *et al.* (2016) evaluated the ultimate strength of SCS sandwich plates and proposed design recommendations to predict the ultimate resistance of these sandwich plates.

Li *et al.* (2017) conducted experimental investigations on a new type of composite slab with lightweight aggregate concrete. A new type of failure mode in the composite members was observed with higher bending capacity and considerable end slip in the long-span slabs. Furthermore, analytical ultimate capacity and the shear bond stress were predicted using the slenderness and force equilibrium methods with reasonable accuracy.

In another study, Li *et al.* (2019) presented an experimental work to evaluate the laminated pouring technique in composite slabs manufactured with lightweight aggregate concrete and polymer fiber reinforced lightweight aggregate concrete with a closed-type steel sheeting profile.

The structural behavior of this system was evaluated by considering the lamination thickness. Their study showed that the proposed technique for lamination did not influence the failure modes. However, using additional fibers could enhance the mechanical interlocking and friction at the steel sheeting-concrete interface.

Sener *et al.* (2014, 2015) investigated the behavior of composite beams under out-of-plane loads. They compared the results of experimental tests with different design codes. Comparisons showed that ACI equations underestimated the out-of-plane flexural strength of SC walls.

The present study is part of ongoing comprehensive research on Steel-Concrete (SC) composite walls. In this research, SC composite walls are considered to be used as retaining walls in deep excavations in tall buildings. First, Sabouri-Ghomi *et al.* (2016) presented a closed-form solution based on partial interaction theory (Wright and Oduyemi (1991)) to analyze the SC composite walls under out-of-plane loads. In the other study, Sabouri-Ghomi *et al.* (2020) performed an experimental program to investigate the behavior of SC composite walls under out-of-plane loads. Nine specimens were tested and the influence of different parameters such as distance between shear connectors, length of shear connectors, concrete compressive strength, use of compressive steel plate and compressive steel reinforcement was investigated.

In the present study, an analytical procedure presented earlier by Sabouri-Ghomi *et al.* (2016) is modified. A new loading condition, as well as a cracked concrete section, is considered in the modified analytical procedure. Force-displacement curves from the improved analytical formulation are compared with those obtained from the experimental tests and numerical simulations. In addition, a FE parametric study is performed in ABAQUS software to investigate the influence of different parameters on the behavior of SC composite walls subjected to out-of-plane loads

2. Analytical procedure

In this section, an improved analytical formulation, which is based on partial interaction theory, to analyze the SC composite walls under out-of-plane loads is presented. The new improved formulation is based on the analytical procedure previously presented by Sabouri-Ghomi *et al.* (2016). In the current improved analytical formulation, a new loading condition- an equilibrium load of soil pressure is applied in the middle of the wall, and the concrete cracking effect is taken into consideration to simulate the real conditions.

2.1 Partial interaction theory to analyze the SC composite walls

Theoretical relations are obtained by considering the flexibility of the connection in the interface of steel plate and concrete. When the loads are applied to the composite walls, the slip takes place between the layers. The amount of this slip depends on the shear stiffness of the connectors (Sabouri-Ghomi *et al.* 2016). To derive the formulations, the retaining wall is assumed as a one-way slab. It is common to use a one-meter strip to derive the formulations for one-way slabs. Also, due to the one-way behavior of the retaining wall, only two edges of the strip are restrained. The effect of adjacent strips in increasing the stiffness is negligible, and it is not taken into account in this study. Therefore, a flexural beam with 1000 mm width, simple supports, and concentrated load is considered. The height of this beam is equal to the wall thickness. Details of the beam-slab strip model are shown in Fig. 2.

Following assumptions are considered for deriving the formulation. The same assumptions were previously assumed by others (Wright and Oduyemi 1991, Sabouri-Ghomi *et al.* 2016):

(1) The materials are elastic.
(2) Deflections are small.
(3) The shear connection between the layers is assumed to act as a continuous connection.
(4) The distribution of strains through the depth of layers is linear.
(5) In every section of the beam, each layer is bent to the same radius of curvature, and no buckling or separation of the layers occurs.
(6) No friction between the layers is considered.
(7) The concrete section is cracked in the tension area.
(8) For simplicity, the steel reinforcements are not considered in the design process, and they are only assumed as thermal steel reinforcements.

The theoretical relations are obtained through the following steps:

The slip between the layers (concrete and steel plate) is obtained as

$$\gamma = \frac{Q}{k} = \frac{qs}{nk} \tag{1}$$

The shear flow is equal to the rate of force changes applied between the layers

$$q = -\frac{dF}{dx} \tag{2}$$

Eq. (2) can be substituted in Eq. (1)

$$\gamma = -\frac{S}{nk}\frac{dF}{dx} \tag{3}$$

The rate of slip changes is equal to the strain difference at the interface of concrete and steel plate

$$\frac{d\gamma}{dx} = -\frac{S}{nk}\frac{d^2F}{dx^2} = \varepsilon_{ct} - \varepsilon_{pc} \tag{4}$$

These strains at the interface of the layers can be obtained by a force and a moment that act on the centroid of each layers, as shown in Fig. 2. The strains are derived from simple bending theory as the following equations

$$\varepsilon_{ct} = -\frac{F}{E_c A_c} + \frac{M_c}{E_c I_c}\left(t_c - \frac{t_{cu}}{2}\right) \tag{5}$$

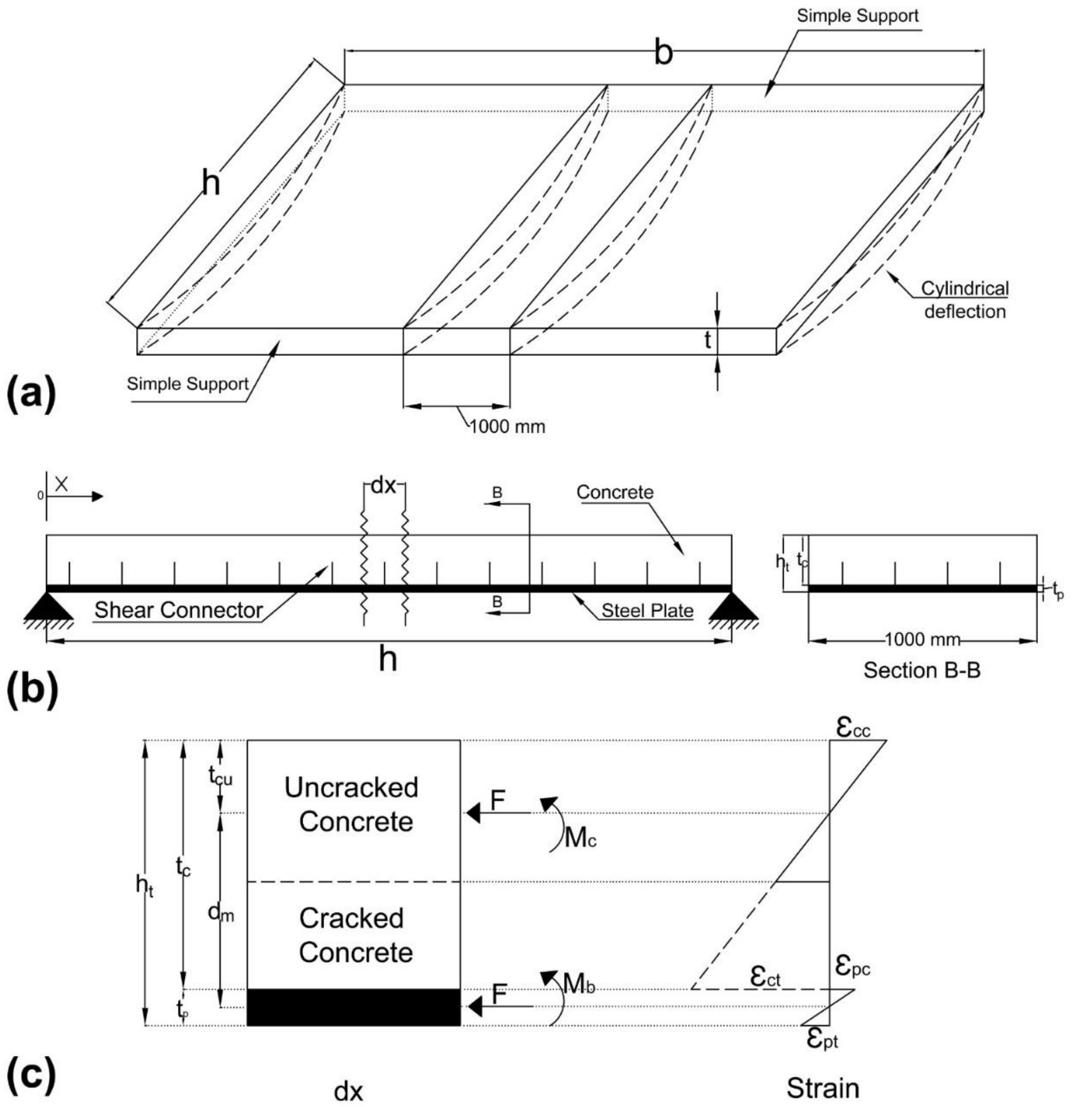

Fig. 2 (a) Slab with simple supports, (b) details of beam-slab strip model, and (c) section along the beam

$$\varepsilon_{pc} = \frac{F}{E_p A_p} - \frac{M_p}{E_p I_p}\left(\frac{t_p}{2}\right) \tag{6}$$

Eqs. (5) and (6) are substituted in Eq. (4) as follows

$$\frac{S}{nk}\frac{d^2F}{dx^2} = \mathrm{F}\left(\frac{1}{E_p A_p} + \frac{1}{E_c A_c}\right) - \frac{M_p}{E_p I_p}\left(\frac{t_p}{2}\right) - \frac{M_c}{E_c I_c}\left(t_c - \frac{t_{cu}}{2}\right) \tag{7}$$

Taking moments around the centroid of the concrete leads to

$$M = M_c + M_p + Fd_m \tag{8}$$

Using the assumption that all the layers are bent to the same curvature, it is possible to write

$$-\frac{d^2y}{dx^2} = \frac{M_c}{E_c I_c} = \frac{M_p}{E_p I_p} = \frac{M_c + M_p}{E_c I_c + E_p I_p} \tag{9}$$

Substituting Eq. (8) in Eq. (9) gives

$$-\frac{d^2y}{dx^2} = \frac{M_c}{E_c I_c} = \frac{M_p}{E_p I_p} = \frac{M - Fd_m}{\sum EI} \tag{10}$$

where

$$\sum EI = E_c I_c + E_p I_p \tag{11}$$

and

$$d_m = t_c - \frac{t_{cu} - t_p}{2} \tag{12}$$

For point-load and simply supported beam, the moment equation is obtained by

$$\begin{Bmatrix} M_L = \dfrac{P}{2}x & for \quad 0 \le x \le h/2 \\ M_R = \dfrac{Ph}{2}(1-\dfrac{x}{h}) & for \quad h/2 \le x \le h \end{Bmatrix} \tag{13}$$

where x is the distance measured from the left support to the differential element in Fig. 2(b). According to Eq. (13), the moment equation varies along the beam. In the following equations, due to perfect symmetry, only the left side of the beam is considered.

Substituting Eqs. (10) and (12) in Eq. (7) gives

$$\frac{S}{nk}\frac{d^2F_L}{dx^2} = F_L\left(\frac{1}{E_pA_p}+\frac{1}{E_cA_c}+\frac{d_m^2}{\Sigma EI}\right) - M_L\left(\frac{d_m}{\Sigma EI}\right) \tag{14}$$

After simplification, Eq. (14) can be written as follows

$$\frac{d^2F_L}{dx^2} - A_1F_L = -A_2M_L \tag{15}$$

where

$$A_1 = \frac{nk}{S}\left(\frac{1}{E_pA_p}+\frac{1}{E_cA_c}+\frac{d_m^2}{\Sigma EI}\right) \tag{16}$$

and

$$A_2 = \frac{nk}{S}\left(\frac{d_m}{\Sigma EI}\right) \tag{17}$$

Using of Eq. (13) and considering the point-load on the beam and simple supported condition, Eq. (15) is solved as

$$F_L = \frac{A_2.P}{2A_1^{1.5}}\left(\frac{e^{(h/2-x)\sqrt{A_1}} - e^{(h/2+x)\sqrt{A_1}}}{1+e^{h\sqrt{A_1}}}\right) + \frac{A_2.P}{2A_1}x \tag{18}$$

With differentiation from Eq. (18) and substitution in Eq. (3), the slip between the layers is obtained as follows

$$\gamma_L = \frac{A_2.P.S}{2n.k.A_1}\left(\frac{e^{(h/2-x)\sqrt{A_1}} + e^{(h/2+x)\sqrt{A_1}}}{1+e^{h\sqrt{A_1}}}\right) - \frac{A_2.P.S}{2n.k.A_1} \tag{19}$$

For calculating the deformed shape of the left side of the beam, simple bending theory is utilized as follows

$$-\frac{d^2y_L}{dx^2} = \frac{M_L - F_Ld_m}{\Sigma EI} \tag{20}$$

Substituting Eqs. (13) and (18) in Eq. (20) gives

$$\frac{d^2y_L}{dx^2} = \frac{F_Ld_m - M_L}{\Sigma EI} = \frac{1}{(\Sigma EI)}\left[\frac{A_2.P.d_m}{2A_1^{1.5}}\left(\frac{e^{(h/2-x)\sqrt{A_1}} - e^{(h/2+x)\sqrt{A_1}}}{1+e^{h\sqrt{A_1}}}\right) + \frac{A_2.P.d_m}{2A_1}x - \frac{P}{2}x\right] \tag{21}$$

With double integration from Eq. (21), the deformed shape of the beam is obtained as follows

$$y_L = \frac{1}{(\Sigma EI)}\left[\frac{A_2.P.d_m}{2A_1^{2.5}}\left(\frac{e^{(h/2-x)\sqrt{A_1}} - e^{(h/2+x)\sqrt{A_1}}}{1+e^{h\sqrt{A_1}}}\right) + \frac{A_2.P.d_m}{12A_1}x^3 - \frac{P}{12}x^3 + C_1x + C_2\right] \tag{22}$$

where C_1 and C_2 are the integration constants and are obtained by boundary conditions. For simply supported beam and point-load, the constants are derived as follows

$$if \quad x=0 \quad \rightarrow \quad y_L = 0 \quad \rightarrow \quad c_2 = 0 \tag{23}$$

$$if \quad x = h/2 \rightarrow y'_L = 0 \rightarrow c_1 = \frac{Ph^2}{16} + \frac{A_2.P.d_m}{2A_1^2} - \frac{A_2.P.d_m.h^2}{16A_1} \tag{24}$$

Substituting Eqs. (23) and (24) in Eq. (22) gives the final equation of beam deformation

$$y_L = \frac{A_2.P.d_m}{2(\Sigma EI).A_1^{2.5}}\left(\frac{e^{(h/2-x)\sqrt{A_1}} - e^{(h/2+x)\sqrt{A_1}}}{1+e^{h\sqrt{A_1}}}\right) + \left(\frac{A_2.P.d_m}{12(\Sigma EI).A_1} - \frac{P}{12(\Sigma EI)}\right)x^3 + \left(\frac{Ph^2}{16(\Sigma EI)} + \frac{A_2.P.d_m}{2(\Sigma EI).A_1^2} - \frac{A_2.P.d_m.h^2}{16(\Sigma EI).A_1}\right)x \tag{25}$$

3. Experimental program

As mentioned previously, Sabouri-Ghomi *et al.* (2020) performed a comprehensive experimental program to

Table 1 Details of SC composite walls tested

Specimens	W1	W2	W4	W5	W6	W7	W8	W9
Length (mm)	1300	1300	350	350	350	350	350	350
Height (mm)	1000							
Plate thickness (mm)	2							
Concrete thickness (mm)	100							
Shear connector spacing (mm)	100	200	100	100	100	100	350	100
Shear connector length (mm)	85	85	85	40	40	85	85	85
Concrete cubic strength (MPa)	28	28	28	28	28	45	28	28
With compressive plate								
With compressive reinforcement								

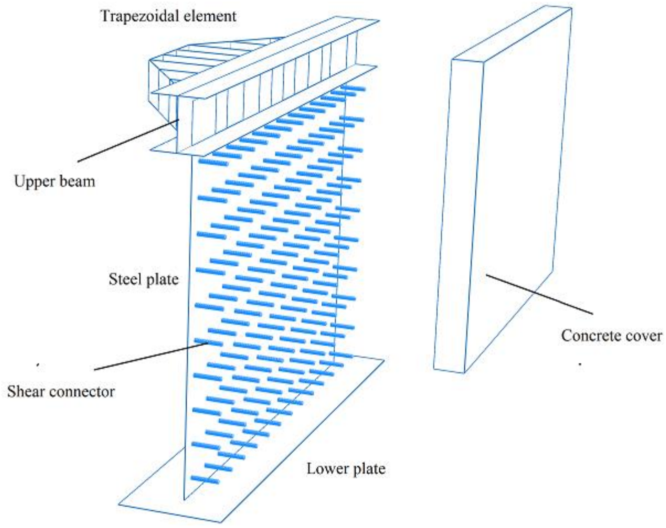

Fig. 3 Schematic of SC composite wall test specimen

Fig. 4 Test set-up details

investigate the behavior of SC composite walls under out-of-plane loads. Table 1 shows the details of the tested SC composite walls. In total, nine specimens (W1 to W9) were considered. In the experimental study, effects of different parameters such as spacing between the shear connectors, length of the shear connectors, concrete ultimate strength, use of compressive steel plate and compressive steel reinforcement were investigated to evaluate their influence

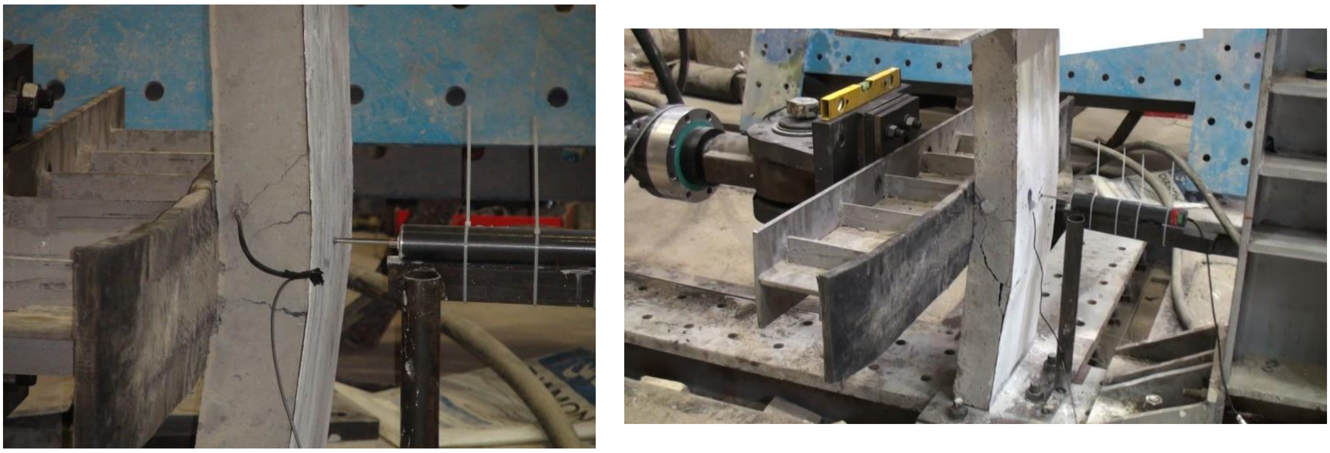

(a) (b)

Fig. 5 Failure modes of specimens, (a) Flexural Failure mode and (b) Shear Failure mode

Table 2 Summary of details of specimens for parametric study

Specimens	W1	W2	W10	W11	W12	W13	W14	W15	W16	W17	W18
Stud spacing (mm)	100	200	150	250	100	100	100	100	100	100	100
Stud length (mm)	80	80	80	80	40	80	80	80	80	80	80
Concrete cubic strength (MPa)	28	28	28	28	28	45	28	28	28	28	28
Plate thickness (mm)	2	2	2	2	2	2	3.5	2	2	2	2
Concrete thickness (mm)	100	100	100	100	100	100	100	125	150	100	100
Wall width (mm)	1300	1300	1300	1300	1300	1300	1300	1300	1300	350	350
Wall height (mm)	1000	1000	1000	1000	1000	1000	1000	1000	1000	1000	2000
Wall's height to thickness ratio	10	10	10	10	10	10	10	8	6.67	10	20
Wall's width to thickness ratio	13	13	13	13	13	13	13	10.4	8.67	3.5	3.5

on the performance of SC composite walls. Fig. 3 shows the schematic of the SC wall test specimen.

The load was applied using a rigid spreader beam in the middle of the specimens. A 50-ton hydraulic actuator with a 300 mm stroke was used to apply the load. Fig. 4 shows the setup of the experimental test. The tested SC composite walls showed a very good behavior under out-of-plane loads in terms of stiffness, strength, and ductility. Both flexural and shear failure modes were observed during the tests (Fig. 5). More details of the experimental work and experimental results can be found elsewhere (Sabouri-Ghomi *et al*. 2020).

4. Finite element analysis of SC composite walls

A finite element model was developed in ABAQUS (Hibbitt *et al.* 2011) to analyze the SC composite walls under out-of-plane load. The accuracy of the FE model has previously been validated by comparing its results with those of experimental specimens (Sabouri-Ghomi *et al.* 2020). The FE study has been extended in this research in order to verify the accuracy of the analytical formulations.

Another important objective for performing further FE simulations was to conduct a detailed parametric study to investigate the effects of different parameters on the behavior of SC composite walls when subjected to out-of-plane loads. Details of the specimens considered for the extended FE study are shown in Table 2.

W1 specimen was considered as a reference of SC composite wall to be compared with other specimens (i.e., W2 and W10 to W18). In these specimens, only one parameter was changed in comparison to W1. The effect of stud spacing on the behavior of SC composite walls was investigated in W2, W10, and W11 specimens. Moreover, W12, W13, and W14 specimens were used to study the influence of stud length, concrete compressive strength, and plate thickness, respectively. Furthermore, the effect of concrete thickness was evaluated in W15 and W16 specimens. At the end, the influence of the wall's width to thickness ratio and the wall's height to thickness ratio was considered in the W17 and W18 specimen.

The FE model had a steel plate, concrete cover, and shear connectors. The steel plate was modeled using linear quadrilateral shell elements (S4R). S4R is a 4-node, quadrilateral, stress/displacement shell element with

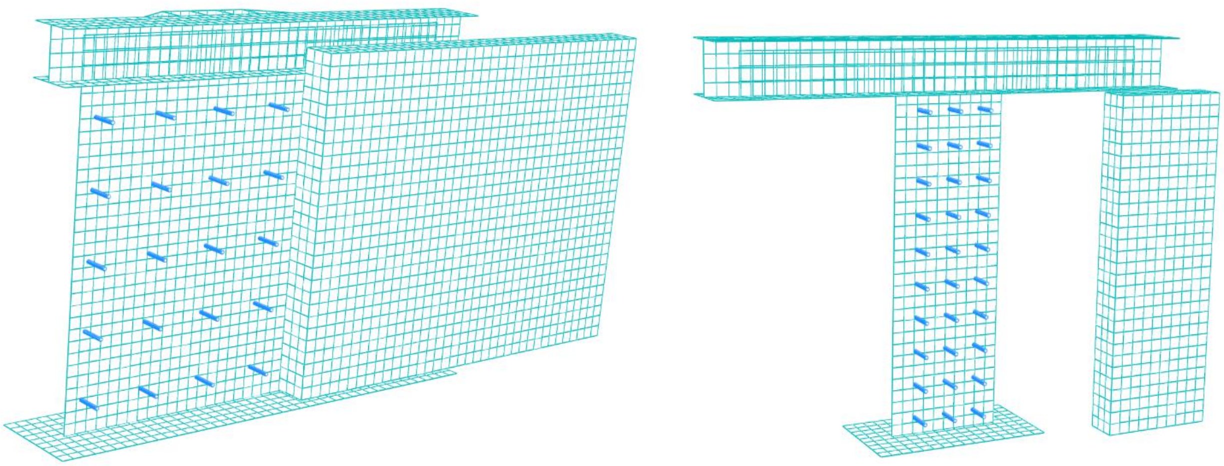

(a) (b)

Fig. 6 The FE model of composite walls (a) W2 specimen and (b)W4 specimen

reduced integration and a large-strain formulation. The concrete was modeled by linear hexahedral solid elements (C3D8R). The C3D8R element is a linear brick element, with reduced integration. Furthermore, shear connectors were modeled by beam elements (B31). B31 is a 2-node linear beam with a single integration point per element (Hibbitt *et al.* 2011).

For the FE analysis, the steel material was modeled using multi-axial plasticity theory with Von-Mises yield criteria. In addition, concrete damage plasticity (CDP) in ABAQUS was utilized to model the behavior of concrete material. The concrete damage plasticity model assumes that the main two failure mechanisms of the concrete material are tensile cracking and compressive crushing. The material parameters to define the CDP models are dilatation angle (ψ), flow potential eccentricity ($\in$), the ratio of the biaxial compressive yield stress to the uniaxial compressive yield stress (σ_{b0}/σ_{c0}) and Kc . In this study, the amount of dilation angle, flow potential eccentricity, stress ratio, and Kc were considered equal to 35°, 0.1, 1.16, and 0.67, respectively.

The concrete compressive curve and flexural tensile strength of concrete were defined using Eq. (26) (Hognestad *et al.* 1955) and Eq. (27) (Ahmed *et al.* 2014)

$$f_c = f_c'\left[\frac{2\varepsilon_c}{\varepsilon_0} - \left(\frac{\varepsilon_c}{\varepsilon_0}\right)^2\right] \tag{26}$$

$$f_r = 0.45\left(f_c'\right)^{2/3} \tag{27}$$

where ε_c is concrete strain and ε_0 is strain when f_c reaches to f_c' and considered equal to 0.002.

To simulate the welded connections, a tie constraint was utilized to avoid any relative movements between the tied elements (Hibbitt *et al.* 2011). Furthermore, the interaction between the steel plate and concrete cover was considered using tangential behavior (frictionless, i.e., the coefficient of friction equal to zero) and normal behavior (hard contact with default properties). Moreover, the shear connectors were embedded inside the concrete with an embedded region constraint in ABAQUS to simulate the interaction between the concrete and the shear connectors.

In finite element analysis, the mesh size plays an important role in the accuracy and efficiency of the results. Therefore, a mesh convergence analysis was conducted to select optimum mesh sizes for concrete cover, steel plate, and shear connectors. It was observed that the meshing refinement was not sensitive after having the maximum mesh size of less than 35 mm for shell and solid elements and 20 mm for beam elements. Fig. 6 shows the FE model of SC composite walls.

5. Results and discussion

In this section, the efficiency of the analytical formulations is evaluated by comparing the results with those of experimental specimens and numerical models. Furthermore, the influence of different parameters on the behavior of SC composite walls such as distance between shear connectors, length of shear connectors, concrete compressive strength, plate and concrete thickness, wall's width to thickness ratio, and wall's height to thickness ratio is numerically investigated.

5.1 Validation of analytical formulations

From the experimental campaign (i.e., W1 to W9), only W1, W2, W4, W5, and W7 specimens were considered as they fulfill the formulation requirements. W8 specimen was not considered, as in the W8 specimen, due to the large distance between the shear connectors, less connectivity exists between the concrete and the steel plate, which does not satisfy the third assumption in section 2. Fig. 7 presents a comparison between the analytical and experimental

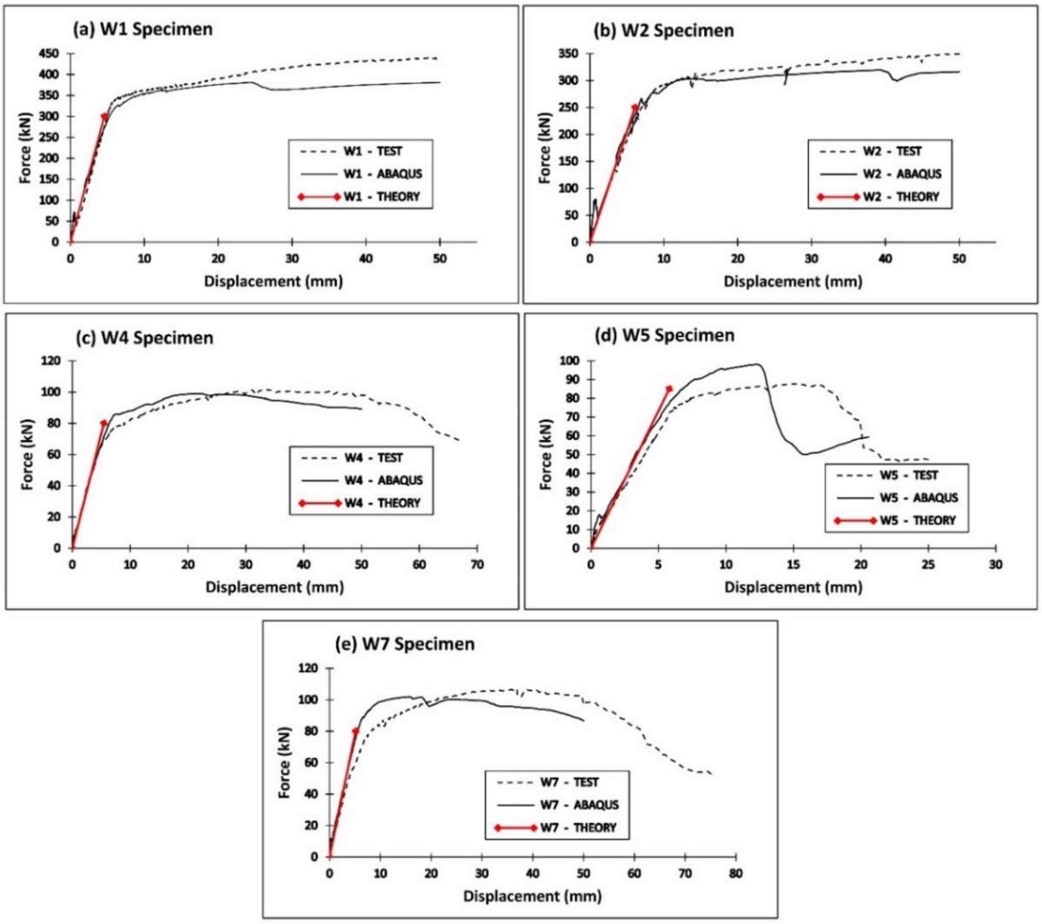

Fig. 7 Force-displacement curve comparison between experimental, numerical and analytical states

results for the selected specimens (Fig. 7). This figure also includes the results of the FE analysis.

The force-displacement curves of specimens in the analytical state were derived based on the proposed partial interaction theory. Considering the assumptions in section 2, the force-displacement curves were plotted using Eq. (25), only in the elastic phase.

It is clear from Fig. 7 that the proposed theoretical formulation has a good capability to predict the out-of-plane behavior of the SC composite walls. In all specimens, at the very beginning of the loading (i.e., elastic phase), the force-displacement curves in the analytical state are in excellent agreement with the numerical and experimental results. For few specimens, due to the non-linearity of the concrete as well as micro-cracking in concrete, slightly lower stiffness is observed in the tests.

As mentioned in the previous section, due to a limited number of experimental specimens, further simulations with more specimens (W10-W18) have been conducted in ABAQUS in order to confirm the accuracy of the proposed analytical procedure. Fig. 8 compares the results of the analytical formulations with those from numerical models. It is obvious from this figure that there is a very good agreement between the analytical and numerical results in W10 to W18 specimens.

5.2 Parametric studies

5.2.1 Effect of shear connectors spacing on the behavior of SC composite walls

To study the effect of distance between shear connectors on the behavior of SC composite walls, the force-displacement curves with different shear connectors spacing (i.e., S=100 mm, S=150 mm, S=200 mm, and S=250 mm for W1, W2, W10, and W11 specimens) were derived from FE analysis. As shown in Fig. 9(a), when the number of shear connectors increased, the strength and stiffness of the SC composite walls were increased, and the yield displacement was decreased. To obtain full composite action, the spacing between the shear connectors must be decreased accordingly. However, a very short spacing between shear connectors is not suitable due to difficulties in welding and for economic considerations. Therefore, a minimum shear connector spacing of 100 mm was considered in the numerical simulation.

It was also observed that by increasing the shear connector spacing to 250 mm (W11 specimen), the SC composite wall failed in small deflection. Unlike the other specimens, this wall failed in a flexural shear failure mode with low ductility. This was due to the extension of the tensile diagonal cracks in the wall section due to the large spacing between the shear connectors (stirrups). It was

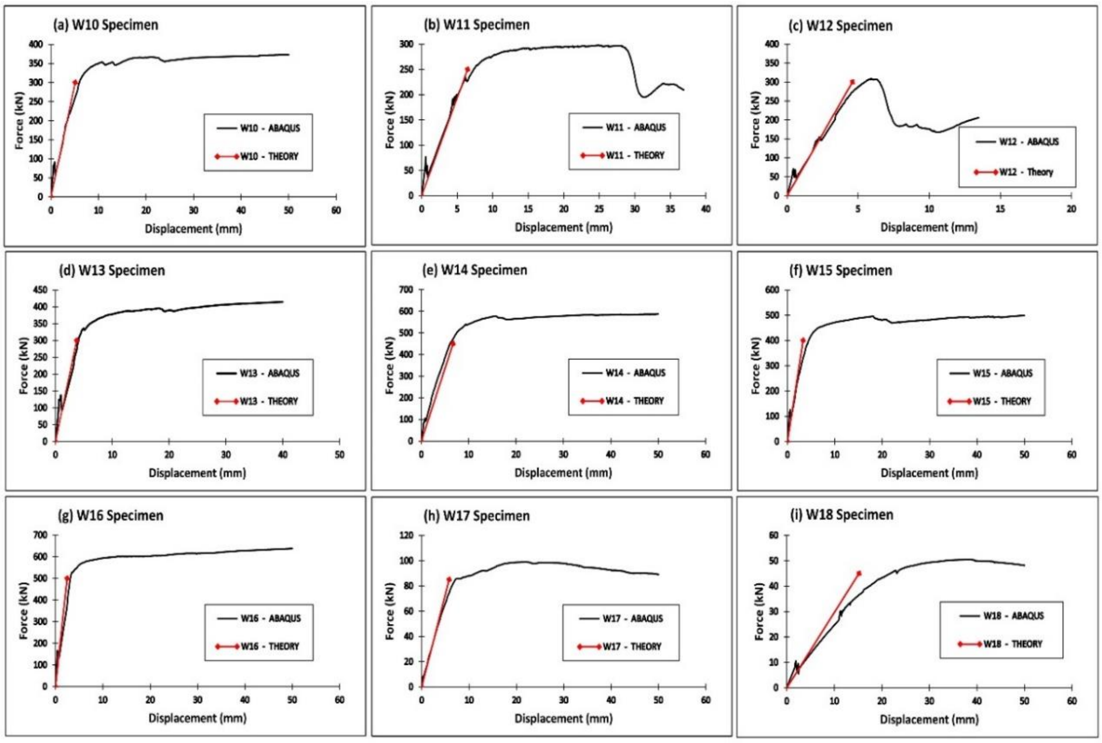

Fig. 8 Force-displacement curves for W10 to W18 specimens

observed that as long as the distance between the shear connectors remained less than or equal to 2d, no shear failure mode was observed in the SC composite walls. Once the spacing between the shear connectors exceeded 2d, tensile diagonal cracks developed, and the shear failure mode was observed in the SC wall.

5.2.2 Effect of shear connectors length on the behavior of SC composite walls

In the composite walls, the shear connectors not only connect the steel plate with the concrete cover but also act as stirrups against the transverse shear in the wall section (Sabouri-Ghomi *et al.* 2020). As shown in Fig. 9(b), when the length of the shear connector was decreased from 80 mm to 40 mm, the failure mode of the SC composite wall was changed from flexural mode to transverse shear mode. In other words, when the length of the stud decreases, the tensile diagonal cracks extend very fast in the SC composite wall. Therefore, the length of studs must be large enough to act as shear stirrups in the SC composite walls.

5.2.3 Effect of concrete compressive strength on the behavior of the SC composite walls

The effect of concrete compressive strength on the behavior of SC composite walls is shown in Fig. 9(c). With an increase in the concrete compressive strength from 28 MPa to 45 MPa, the strength and stiffness of the SC composite walls were increased. However, according to Fig. 9(c), the increase in the concrete compressive strength does not have a considerable effect on the behavior of composite walls.

5.2.4 Effect of concrete and plate thickness on the behavior of SC composite walls

To investigate the effect of steel plate thickness and concrete thickness, three more specimens were analyzed in the ABAQUS software. The W14 specimen with a plate thickness of 3.5 mm was simulated and compared to the W1 specimen with a plate thickness of 2 mm. Results indicated that with the increase in the plate thickness, the load capacity of the wall increased from 381 kN to 587 kN (about 54 percent). Furthermore, the elastic stiffness of the wall was increased accordingly. This is shown in Fig. 9(d).

In addition, to investigate the effect of concrete thickness, W15 and W16 specimens were modelled and analyzed with a concrete thickness of 125 mm and 150 mm, respectively. The results were compared with W1 specimen with a concrete thickness of 100 mm. It was observed that with the increase of concrete thickness from 100 mm to 125 mm and 150 mm, the load capacity of the wall increased by about 30 percent and 67 percent for the W15 and the W16 specimens, respectively. In other words, the capacity of the wall increased from 381 kN for the W1 specimen to 499 kN and 638 kN for the W15 and W16 specimens, respectively. This observation is presented in Fig. 9(e).

5.2.5 Effect of wall's width to thickness ratio and wall's height to thickness ratio on the behavior of SC composite walls

To study the effect of the wall's width to thickness ratio and the wall's height to thickness ratio, W17 and W18 specimens were analyzed in ABAQUS. In these specimens, the thickness of the concrete and steel plate was constant and only the width and height of the wall were changed. In

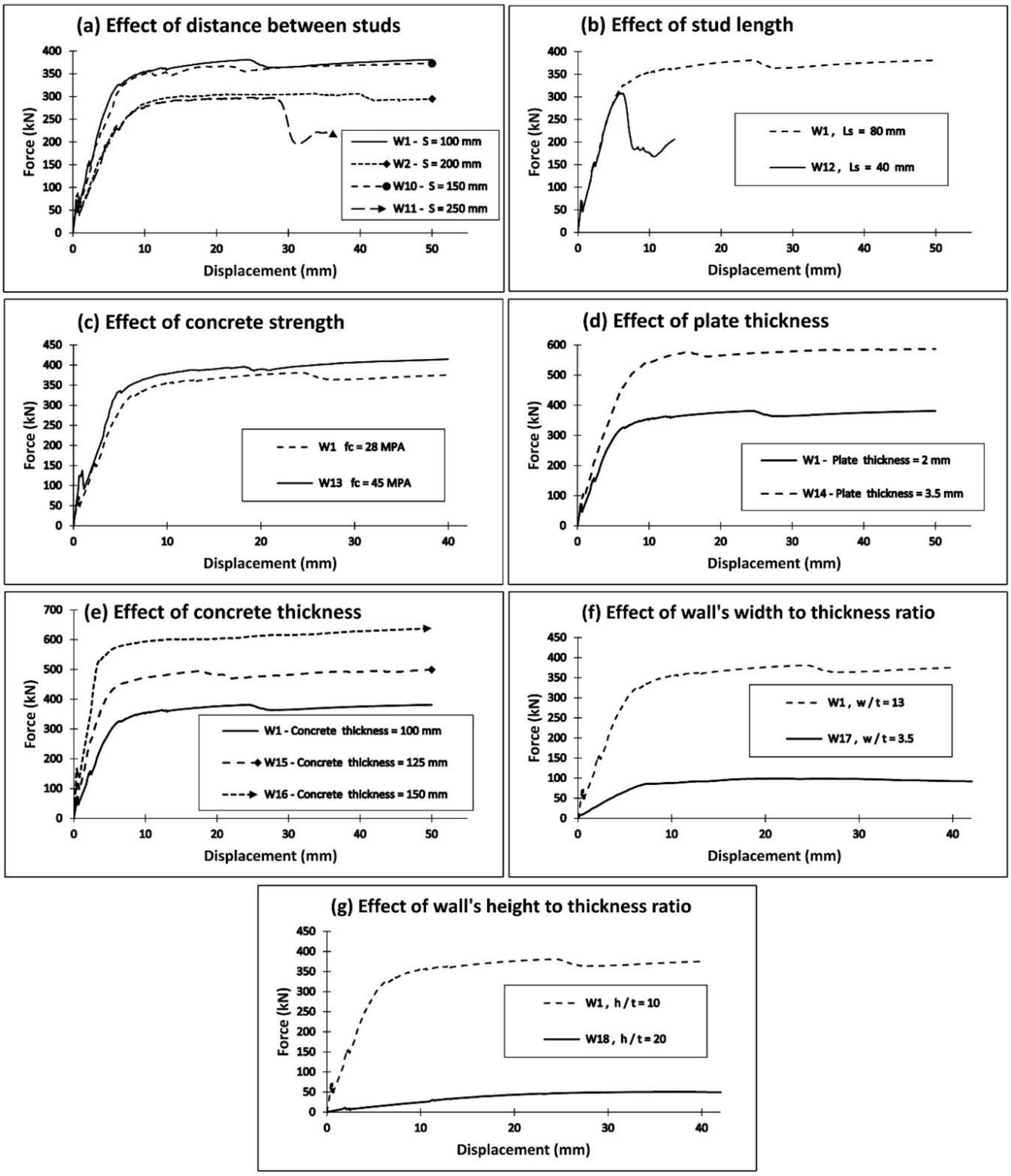

Fig. 9 Effects of different parameters on the behavior of SC composite wall

the W17 specimen in comparison to W1, the wall's width to thickness ratio was reduced from 13 to 3.5. Also, in the W18 specimen in comparison to W17, the wall's height to thickness ratio was increased from 10 to 20. Effects of width to thickness ratio and height to thickness ratio on the behavior of the SC composite walls are shown in Figs. 9(f) and 9(g). According to Fig. 9(f), by reducing the wall's width to thickness ratio, the yielding load, elastic stiffness, and ultimate load capacity are decreased. Also, as shown in Fig. 9(g), the yielding load, elastic stiffness, and ultimate load capacity decrease when the wall's height to thickness ratio is increased.

6. Conclusions

Steel-Concrete (SC) composite system has recently been proposed to use as retaining walls by the authors. In this paper, an improved analytical formulation was proposed to analyze SC composite walls. The analytical formulation is based on partial interaction theory and accounts for cracking in concrete in tension to simulate the real conditions.

The force-displacement curves obtained from several experimental tests were compared with results obtained from the proposed analytical formulation. Due to the limited number of experimental specimens, more specimens with different geometry were modeled and analyzed in ABAQUS software. It was observed that the proposed closed-form solution has a good capability to predict the force-displacement curve of SC composite walls in the elastic phase. In addition, a detailed parametric study was conducted using FE analysis to investigate the effects of different parameters on SC composite walls subjected to out-of-plane load. Seven different parameters (i.e., shear connectors spacing, length of shear connectors, concrete compressive strength, steel plate thickness, concrete thickness, wall's width to thickness ratio, and wall's height to thickness ratio) were considered. The results of the parametric study are summarized as follows:

1-With an increase in the distance between shear connectors beyond 2d, tensile diagonal cracks were developed in the specimens.

2-With a decrease in the length of the shear connector, the failure mode was changed from flexural to the transverse shear failure mode.

3-Increasing the compressive strength of the concrete did not have a significant effect on the strength and stiffness of the SC composite walls.

4-With an increase in the plate thickness and concrete thickness, the wall capacity was increased significantly.

5-With decrease in the wall's width to thickness ratio (the thickness of the wall was kept constant), the ultimate load, yield load, and stiffness of the wall were decreased. Similar behavior was observed when the wall's height to thickness ratio was increased.

References

Ahmed M, Hadi KM, Hasan MA, Mallick J, Ahmed A (2014), "Evaluating the co-relationship between concrete flexural tensile strength and compressive strength", *Int J Struct Eng*, 5(2), 115-131.

Cas B, Bratina S, Saje M, Planinc I (2004), "Non-linear analysis of composite steel-concrete beams with incomplete interaction", *Steel Compos. Struct., Int. J*, 4(6), 489-507. https://doi.org/10.12989/scs.2004.4.6.489.

Ding FX, Liu J, Liu XM, Guo FQ, Jiang LZ (2016), "Flexural stiffness of steel-concrete composite beam under positive moment", *Steel Compos. Struct., Int. J*, 20(6), 1369-1389. http://dx.doi.org/10.12989/scs.2016.20.6.1369.

Dogan O, Roberts TM (2010), "Comparing experimental deformations of steel-concrete-steel sandwich beams with full and partial interaction theories*", Int J of Phys Sci*, 5(10), 1544-1557.

Fanaie N, Esfahani FG, Soroushnia S (2015), "Analytical study of composite beams with different arrangements of channel shear connectors", *Steel Compos. Struct., Int. J*, 19(2), 485-501. http://dx.doi.org/10.12989/scs.2015.19.2.485.

Hibbitt, D., Karlsson, B. and Sorenson, P. (2011), "Simulia ABAQUS 6.11 Users' Manual".

Hognestad E, Hanson NW, McHenry D (1955), "Concrete stress distribution in ultimate strength design", *In Journal Proceedings*, 52(12), 455-480.

Li, X., Zheng, X., Ashraf, M. and Li, H (2017). "Experimental study on the longitudinal shear bond behavior of lightweight aggregate concrete–Closed profiled steel sheeting composite slabs". *Construction and Building Materials*, *156*, 599-610. https://doi.org/10.1016/j.conbuildmat.2017.08.108.

Li, X., Zheng, X., Ashraf, M. and Li, H (2019). "The longitudinal shear bond behavior of an innovative laminated fiber reinforced composite slab". *Construction and Building Materials, 215,* 508-522. https://doi.org/10.1016/j.conbuildmat.2019.04.153.

Liew JR, Sohel KM (2009), "Lightweight steel–concrete–steel sandwich system with J-hook connectors*", Eng Struct,*, 31(5),1166-1178. https://doi.org/10.1016/j.engstruct.2009.01.013.

Oduyemi TO, Wright HD (1989), "An experimental investigation into the behavior of double-skin sandwich beams", *J Constr Steel Res,* 14(3), 197-220. https://doi.org/10.1016/0143-974X(89)90073-4.

Qin Y, Shu GP, Zhou GG, Han JH (2019), "Compressive behavior of double skin composite wall with different plate thicknesses*", J Constr Steel Res*, 157, 297-313. https://doi.org/10.1016/j.jcsr.2019.02.023.

Ranzi G (2006), "Short-and long-term analyses of composite beams with partial interaction stiffened by a longitudinal plate", *Steel Compos. Struct., Int. J,* 6(3), 237-255. https://doi.org/10.12989/scs.2006.6.3.237.

Ranzi G, Bradford MA, Uy B (2003), "A general method of analysis of composite beams with partial interaction", *Steel Compos. Struct., Int. J*, 3(3), 169-184. https://doi.org/10.12989/scs.2003.3.3.169.

Sabouri-Ghomi S, Jahani Y, Bhowmick AK (2016), "Partial interaction theory to analyze composite (steel–concrete) shear wall systems under pure out-of-plane loadings", *Thin Walled Struct*, 104, 211-224. https://doi.org/10.1016/j.tws.2016.03.013.

Sabouri-Ghomi S, Nasri A, Jahani Y, Bhowmick AK (2020), "Flexural performance of composite walls under out-of-plane loads" *Steel Compos. Struct., Int. J*, 34(4), 525-545. DOI: https://doi.org/10.12989/scs.2020.34.4.525.

Sener KC, Varma AH (2014), "Steel-plate composite walls: Experimental database and design for out-of-plane shear", *J Constr Steel Res*, 100, 197-210, https://doi.org/10.1016/j.jcsr.2014.04.014.

Sener KC, Varma AH, Ayhan D (2015), "Steel-plate composite (SC) walls: Out-of-plane flexural behavior, database, and design", *J Constr Steel Res*, 108, 46-59. https://doi.org/10.1016/j.jcsr.2015.02.002.

Sohel KM, Liew JR (2011), "Steel–Concrete–Steel sandwich slabs with lightweight core—Static performance*", Eng Struct,* 33(3), 981-992. https://doi.org/10.1016/j.engstruct.2010.12.019.

Solomon SK, Smith DW, Cusens AR (1976), "Flexural tests of steel-concrete-steel sandwiches*", Mag Concrete Res*, 28(94), 13-20. https://doi.org/10.1680/macr.1976.28.94.13.

Subedi NK, Coyle NR (2002). "Improving the strength of fully composite steel-concrete-steel beam elements by increased surface roughness—an experimental study" *Eng Struct.;* 24(10):1349-55. https://doi.org/10.1016/S0141-0296(02)00070-6.

Vasdravellis G, Uy B, Tan EL, Kirkland B (2012). "Behavior and design of composite beams subjected to negative bending and compression". *J Constr Steel Res*. 79:34-47. https://doi.org/10.1016/j.jcsr.2012.07.012.

Wright HD, Oduyemi TO (1991). "Partial interaction analysis of double skin composite beams.*" J Constr Steel Res.* 19(4), 253-83. https://doi.org/10.1016/0143-974X(91)90019-W.

Xie M, Foundoukos N, Chapman JC (2005). "Experimental and numerical investigation on the shear behavior of friction-welded bar–plate connections embedded in concrete." *J Constr Steel Res,* 61(5):625-49. https://doi.org/10.1016/j.jcsr.2004.10.005.

Xie M, Foundoukos N, Chapman JC (2007), "Static tests on steel–concrete–steel sandwich beams", *J Constr Steel Res*, 63(6), 735-

750. https://doi.org/10.1016/j.jcsr.2006.08.001.

Yan JB, Liew JR (2016). "Design and behavior of steel–concrete–steel sandwich plates subject to concentrated loads". *Compos Struct,* 150:139-52. https://doi.org/10.1016/j.compstruct.2016.05.004.

Yan JB, Liew JR, Zhang MH (2014), "Tensile resistance of J-hook connectors used in Steel-Concrete-Steel sandwich structure", *J Constr Steel Res,* 100, 146-162. https://doi.org/10.1016/j.jcsr.2014.04.023.

Yan JB, Liew JR, Zhang MH, Sohel KM (2015), "Experimental and analytical study on ultimate strength behavior of steel–concrete–steel sandwich composite beam structures", *Mater Struct,* 48(5), 1523-1544. https://doi.org/10.1617/s11527-014-0252-4.

Yan JB, Wang XT, Wang T (2018), "Compressive behavior of normal weight concrete confined by the steel face plates in SCS sandwich wall", *Constr Build Mater*, 171, 437-454. https://doi.org/10.1016/j.conbuildmat.2018.03.143.

Yan JB, Wang Z, Wang T, Wang XT (2018). "Shear and tensile behaviors of headed stud connectors in double skin composite shear wall". *Steel Compos. Struct., Int. J.* 26(6):759-69. https://doi.org/10.12989/scs.2018.26.6.759.

DL

Nomenclature

γ	Slip between the layers	T	Thickness; subscripts c for concrete, p for steel plate and cu for uncracked concrete
Q	Load on one shear connector	h_t	Total depth of beam section
q	Shear flow	P	pointed load on beam
S	distance between shear connectors	Y	Vertical deflection of the beam
n	Number of shear connectors in cross section of beam	F_{yp}	Yield stress of steel faceplate
k	Stiffness of one shear connector	F_{us}	Ultimate tensile strength of the shear connector
A	Area; subscripts c for concrete, p for steel plate and s for shear connectors	f_c'	Cylindrical compressive strength of the concrete
F	Force between layers	h_s	Height of shear connector
ε_{ct}	Concrete strain in tension region	H	Height of the composite wall (span of beam)
ε_{pc}	Steel plate strain in compression region	d	Effective depth of the cross section
M	Bending moment; subscripts c for concrete and p for steel plate	B	Length of the composite wall
E	Modules of elasticity; subscripts c for concrete and p for steel	d_s	Shear connector diameter
I	Second moment of area, subscripts c for concrete and p for steel plate		